Proc. Natl. Acad. Sci. USA
Vol. 88, pp. 11569–11573, December 1991
Neurobiology

Synaptic background activity influences spatiotemporal integration in single pyramidal cells

(time constant/input resistance/intracellular recording/synaptic integration)

ÖJVIND BERNANDER*, RODNEY J. DOUGLAS*†, KEVAN A. C. MARTIN†, AND CHRISTOF KOCH*‡

*Computation and Neural Systems Program, California Institute of Technology, Pasadena, CA 91125; and †Medical Research Council Anatomical Neuropharmacology Unit, Oxford OX1 3QT, United Kingdom

Communicated by Francis Crick, September 9, 1991 (received for review June 5, 1991)

ABSTRACT **The standard one-dimensional Rall cable model assumes that the electrotonic structure of neurons does not change in response to synaptic input. This model is used in a great number of both theoretical and anatomical-physiological structure–function studies. In particular, the membrane time constant, τ_m, the somatic input resistance, R_{in}, and the electrotonic length are used to characterize single cells. However, these studies do not take into account that neurons are embedded in a network of spontaneously active cells. Synapses from these cells will contribute significantly to the membrane conductance, especially if recent evidence of very high specific membrane resistance, $R_m = 100$ kΩ·cm², is taken into account. We numerically simulated the electrical behavior of an anatomically reconstructed layer V cortical pyramidal cell receiving input from 4000 excitatory and 1000 inhibitory cells firing spontaneously at 0–7 Hz. We found that, over this range of synaptic background activity, τ_m and R_{in} change by a factor of 10 (80–7 msec, 110–14 MΩ) and the electrotonic length of the cell changes by a factor of 3. We show that this significantly changes the response of the cell to temporal desynchronized versus temporal synchronized synaptic input distributed throughout the neuron. Thus, the global activity of the network can control how individual cells perform spatial and temporal integration.**

Conventional one-dimensional cable theory studies the voltage behavior in active or passive, spatially extended cable structures in response to current injections or synaptic inputs. These models usually assume a uniform membrane resistance, R_m, of 5–10 kΩ·cm² and a small number of synapses. Each synaptic input induces a transient increase in the membrane conductance, but their total conductance is small relative to $G_m = 1/R_m$. However, neurons do not exist in isolation but are embedded in a heavily interconnected network of neurons that are spontaneously active: in the case of visual cortex at rates between 0 and 5 Hz (1, 2). Given that the average cortical pyramidal cell receives input from on the order of 10,000 synapses (3), this synaptic background activity causes an added membrane conductance, G_{syn}, comparable to G_m. In the light of recent evidence suggesting much higher values for R_m (4, 5), G_{syn} may actually constitute the main bulk of the effective membrane conductance, $G_{m,eff}$ (the sum of G_m and G_{syn}). Since both input resistance, R_{in}, and time constant, τ_m, depend strongly on $G_{m,eff}$, we expect the overall activity level of the network to determine integrative properties of cells. Previously, a simple model was used (6) to study the effect synaptic background activity has on the efficiency of single synapses in α motoneurons, whereas Holmes and Woody (7) investigated the impact of a nonhomogeneous synaptic distribution on synaptic efficiency. In this paper we study the overall effect of synaptic background activity on the spatial and temporal integrative properties of individual pyramidal cells and discuss the functional implications of our results, both for interpreting data from an *in vitro* (e.g., slice or culture) preparation as well as for cortical information processing strategies.

The publication costs of this article were defrayed in part by page charge payment. This article must therefore be hereby marked "*advertisement*" in accordance with 18 U.S.C. §1734 solely to indicate this fact.

MODEL

A typical layer V pyramidal cell (Fig. 3) in striate cortex was filled with horseradish peroxidase during *in vivo* experiments in the anesthetized, adult cat (8). The somatic input resistance of this neuron was $R_{in} = 23$ MΩ, and its time constant was $\tau_m = 20$ msec. The three-dimensional coordinates and diameters of the dendritic tree were measured by a computer-assisted method, and each branch was replaced by a single equivalent cylinder. This morphological data was fed into a modified version of NEURON, an efficient single-cell simulator developed by Hines (9). Neocortical pyramidal cells are covered with 5000–15,000 dendritic spines (3, 10). We assumed that our cell receives excitatory input from 4000 synapses of the non-*N*-methyl-D-aspartate type. The time course of the associated conductance increase was modeled by an α function:

$$g(t) = \text{const} \cdot te^{-t/t_{peak}}, \quad [1]$$

with const $= g_{peak}e/t_{peak}$. This conductance increase peaks at $t_{peak} = 1.5$ msec and is over within 10 msec (Fig. 1*B*; refs. 11 and 12). The density of excitatory synapses per unit area is very small at or near the soma, reaches 50% of its peak value 40 μm away from the soma, and levels out to a constant value after about 70 μm away from the soma, in agreement with anatomical data (13). We accounted for excitatory synapses onto dendritic spines by absorbing them into the cable structure (14, 15). About 20% of all synapses on a pyramidal cell are believed to be inhibitory. Accordingly, our cell received 1000 inhibitory synapses, 500 synapses of the Cl^--permeable γ-aminobutyric acid type A ($GABA_A$) and 500 of the K^+-permeable GABA type B ($GABA_B$). Their time courses were modeled by α functions (Eq. 1), but with larger values of t_{peak} (see legend of Fig. 1). The density of $GABA_A$ synapses peaked at the soma and decayed over 200 μm, whereas the density of $GABA_B$ synapses peaked 50 μm away from the soma and decayed to a small constant value with increasing distance from the soma. All synapses were independently activated at random (using a Poisson distribution) at a rate of f Hz. We initially ran our simulations with $5000f$ discrete, time-varying synaptic inputs per sec. However, given the large number of synapses, we replaced $g_{syn}(t)$ in each branch by an equivalent time-averaged conductance input. Given a compartment containing n synapses, we

Abbreviations: GABA, γ-aminobutyric acid; EPSP, excitatory postsynaptic potential.

‡To whom reprint requests should be addressed at: Division of Biology, 216-76, California Institute of Technology, Pasadena, CA 91125.

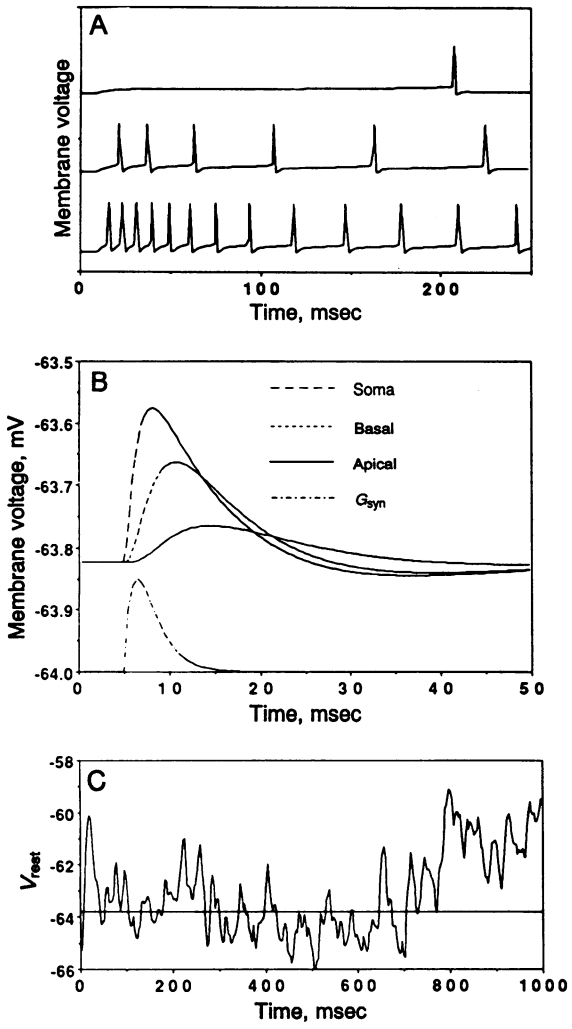

FIG. 1. Somatic potential of our simulated layer V pyramidal cell in response to different current inputs for f = 1 Hz. (*A*) Upon injection of a current step of 0.4 nA (top trace), the cell fires an action potential. The threshold for spike initiation is about −49 mV. The response is delayed by more than 100 msec due to the presence of I_A. The middle and bottom traces show the responses to 0.7- and 1.0-nA current steps, respectively. The calcium-dependent potassium current, $I_{K(Ca)}$, is primarily responsible for the adaptation of the firing frequency. (*B*) Postsynaptic potential in response to a single excitatory synapse at three different locations (soma, middle of the basal tree, and middle of the apical tree). Since the g_{peak} associated with each synapse is constant (0.5 nS), the peak voltage decreases with increasing distance and peaks later. Notice the small amplitude of this "unitary" EPSP. The time course of the excitatory conductance input $g(t)$ is plotted at the bottom of the figure and is given by $g(t) = g_{peak} \cdot (t/t_{peak}) e^{1 - t/t_{peak}}$, with g_{peak} = 0.5 nS, t_{peak} = 1.5 msec, and a synaptic reversal potential E_{syn} = 0 mV. (*C*) The somatic potential of the cell in response to the random 1-Hz activity of all 5000 synapses at f = 1 Hz. The horizontal lines indicate the voltage when the time-averaged synaptic input of Eq. 2 is used. The time course of the inhibitory conductance changes are described by the above $g(t)$ function, with g_{peak} = 1.0 nS, t_{peak} = 10 msec, and E_{syn} = −70 mV for $GABA_A$ and g_{peak} = 0.1 nS, t_{peak} = 40 msec, and E_{syn} = −95 mV for the $GABA_B$ synapses. The parameters characterizing the passive dendrites are R_m = 100 kΩ·cm², C_m = 1 μF/cm², R_i = 200 Ω·cm, and E_{leak} = −66 mV (4, 14, 19, 20). The cell body contains seven voltage-dependent ionic currents: two sodium currents (I_{Na} with a peak conductance $\bar{g}_{Na}$ = 200 mS/cm² and I_{Na-p} with $\bar{g}_{Na-p}$ = 1, E_{Na} = 50 mV), one calcium current (I_{Ca} with $\bar{g}_{Ca}$ = 1, E_{Ca} = 115 mV), and four potassium currents with E_K = −95 mV (I_{DR} with $\bar{g}_{DR}$ = 120, I_A with $\bar{g}_A$ = 1, I_M with $\bar{g}_M$ = 0.6, and the calcium-dependent $I_{K(Ca)}$ with $\bar{g}_{K(Ca)}$ = 45 mS/cm²). Calcium buffering and diffusion was modeled by a first-order exponential decay with a time constant of 200 msec. Since adding an axon to our cell made little difference to its electrical behavior, we left it out. Simulations usually involved between 164 and 820 spatial compartments. The simulator (discussed in ref. 9) uses a second-order Crank–Nicholson integration method and typically runs 60 sec on a SUN Sparc II workstation to simulate 100 msec of the complete model.

defined an equivalent membrane conductance for each synaptic input type

$$G_{m,eff} = \bar{g}_{syn} f n, \quad [2]$$

where $\bar{g}_{syn} = \int g(t)dt = e t_{peak} g_{peak}$. This decreased computation time dramatically without changing the behavior of the cell (Fig. 1*C*). The dendrites are assumed to be passive, with R_m = 100 kΩ·cm² (4, 5, 14). The final effective membrane conductance is obtained by adding all the different synaptic components to the leak conductance. At f = 1 Hz, the effective R_m varies between 6 and 35 kΩ·cm², depending on the specific compartment. Notice the trade-off between the peak conductance change, time to peak, the number of synapses, and the spontaneous background frequency.

The cell body contains seven different ionic currents, modeled using Hodgkin–Huxley-like kinetics with voltage-independent time constants (ref. 16; see legend of Fig. 1), including a fast (as well as a sustained) sodium current underlying spike generation, a high-threshold, L type, calcium current, and four potassium currents (I_A, I_M, I_{DR}, $I_{K(Ca)}$). All these currents have been characterized in cortical cells (17, 18). The dynamics of free, intracellular calcium was approximated by a single intracellular compartment at the soma.

RESULTS

The basic performance of the neuron for a synaptic background activity of 1 Hz is illustrated in Fig. 1. The response of the cell to a long-lasting current input (Fig. 1*A*) shows the spike adaptation typical of regular-spiking pyramidal cells (21). Adaptation was usually complete after 100–150 msec. The cell could discharge at rates up to 300 Hz for large current injections (3 nA). Somatic excitatory postsynaptic potentials (EPSPs) caused by a single excitatory synapse are shown in Fig. 1*B* for three different input locations. The size and width of these EPSPs are in good agreement with those recorded in pyramidal cells when intracellularly stimulating a neighboring pyramidal cell (22). Fig. 1*C* illustrates the somatic potential in the presence of the spontaneous background firing. For f = 0.5 Hz, the resting potential stabilizes at around V_{rest} = −65 mV, with τ_m = 22 msec and R_{in} = 21 MΩ, describing the behavior of some of our intracellularly recorded *in vivo* cat pyramidal cells in response to electrical stimuli quite well (8, 18).

Figs. 2 and 3 illustrate what happens if the synaptic background activity is varied. In the absence of any synaptic input, R_{in} = 110 MΩ and τ_m = 80 msec, while the resting potential stabilizes between E_{leak}, the reversal potential of the membrane leak, and E_K, the reversal potential of K^+. In the absence of any synaptic activity, the leak conductance of the dendritic tree contributes about 59% (i.e., 5.3 nS) toward the somatic input conductance, $G_{in} = 1/R_{in}$; the remainder comes from the two potassium currents, I_M and I_A. At 1 Hz background activity, on average five synaptic events are impinging on the cell every msec, contributing a total of 24 nS (34%) to the somatic input conductance G_{in}. Because of the reversal potential of the excitatory synapses (0 mV), the membrane potential throughout the cell is pulled toward more depolarizing potentials, activating additional I_A and I_M currents. Although these trends continue as f is increased, the largest change can be observed between 0 and 2 Hz.

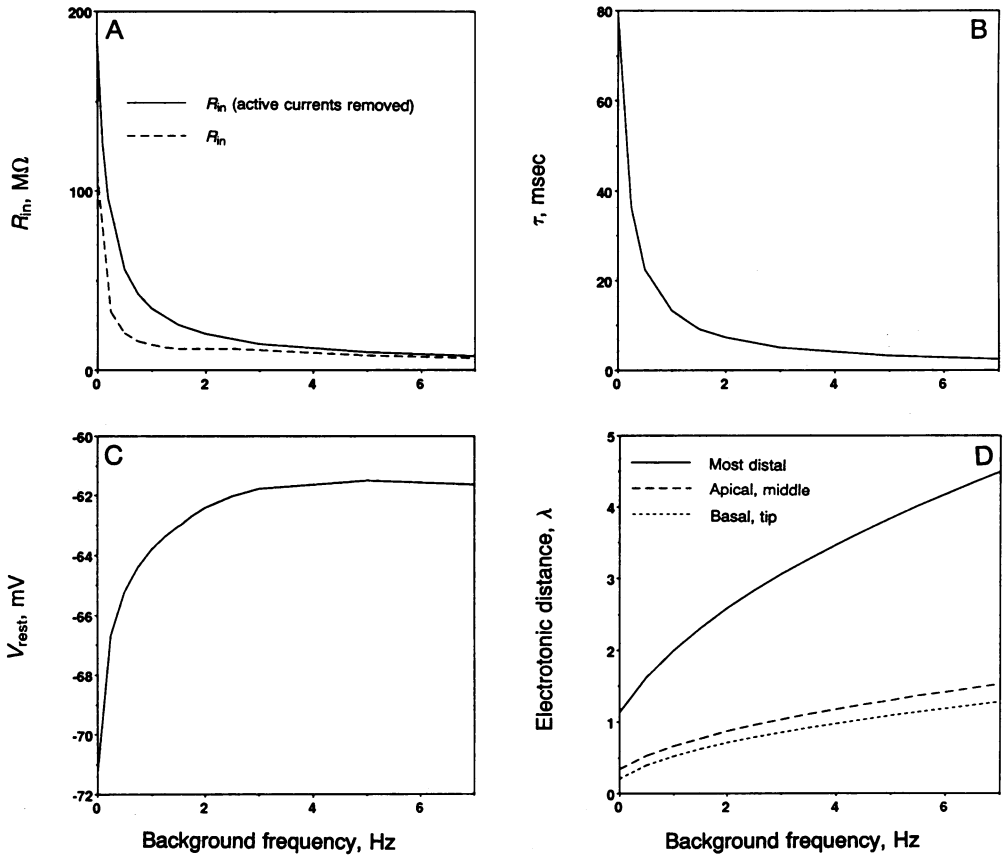

FIG. 2. Impact of synaptic background frequency on cell parameters. (*A*) Somatic input resistance, R_{in}, in the absence of any active currents (top curve; passive neuron) and in our standard model (bottom curve). The former case is analogous to using a Cs^+-filled electrode to block the potassium currents. R_{in} was measured by computing the amplitude of a current step necessary to hyperpolarize the cell body by 1 mV. (*B*) Membrane time constant, τ_m. Since in principle no simple exponential can be fitted to the voltage trajectory in the presence of voltage-dependent currents, we replaced the different currents (in particular, I_M and I_A) by their steady-state values at the resting potential. The somatic potential in response to a small current step was then fitted by two exponentials. We identified the slower component with τ_m. (*C*) Resting potential, V_{rest}, at the cell body. Because active synapses are spread throughout the cell at locations with different input resistances, the resting potential will vary throughout the cell. (*D*) Electrotonic distance, *L*, from the soma to three different locations (the distal end of a basal dendrite, a point halfway up the apical tree, and the most distal point in layer I). *L* was computed as the sum of all branch segments on the path between the location and the soma.

Activating the synaptic input has two distinct effects: the conductance of the postsynaptic membrane increases and the membrane potential is pulled toward the synaptic reversal potential. The system can, at least in principle, independently control these two effects by differentially varying the spontaneous firing frequencies of excitatory versus inhibitory inputs. Thus, increasing f only for the $GABA_B$ inhibition will further increase the membrane conductance but move the resting potential toward more hyperpolarizing potentials.

Varying the synaptic background activity can have a significant impact on the electrotonic structure of the cell (Fig. 3). We plot the electrotonic distance of any particular point from the cell body—that is, the sum of the electrotonic lengths $L_i = \Sigma_j(l_j/\lambda_j)$ associated with each dendritic segment i, where λ_j is the electrotonic length constant of compartment j, l_j is its anatomical length, and the sum is taken over all compartments between the soma and compartment i (24). Increasing the synaptic background activity from $f = 0$ to $f =$ 2 Hz has the effect of stretching the "distance" of any particular synapse to the soma by a factor of about 3, on average. Thus, while a synapse in layer I has an associated *L* value of about 2.6 at 2 Hz, it shrinks to 1.2 if all network activity is shut off, while for a synapse at the tip of a basal dendrite, *L* shrinks from 0.7 to 0.2. In fact, the EPSP induced by a single excitatory synapse at that location goes from 151 to 39 μV, a decrease of about 4. Thus, when the overall network activity is low, synapses in the superficial layer of the cortex could have a significant effect on somatic discharge, while having only a weak modulatory effect on the soma if the overall network activity is high. Note that basal dendrites, which receive a larger number of synapses, stretch more than apical dendrites.

That the synaptic background activity can also modify the temporal integration behavior of the cell is demonstrated in Fig. 4. At any particular background frequency f, we compute the minimal number of additional excitatory synapses (at $g_{peak} = 0.5$ nS) necessary to generate at least one action potential. These synapses were distributed randomly throughout the cell according to the distribution described above. We compare the case in which all synapses are activated simultaneously with the case in which the inputs arrive asynchronously, smeared out over 25 msec (Fig. 4*A*). If $f = 0$, it requires 115 synapses firing simultaneously to generate a single action potential, whereas 145 are needed if the input is desynchronized. This small difference between inputs arriving synchronized and at random is due to the long integration period of the cell. If the background activity increases to $f = 1$ Hz, 113 synchronized synaptic inputs—spread out all over the cell—are sufficient to fire the cell. If, however, the synaptic input is spread out over 25 msec, 202 synapses are now needed in order to trigger a response from the cell. This is mainly due to the much smaller value of τ_m relative to the period over which the synaptic input is spread out. Note that the difference in number of simultaneous

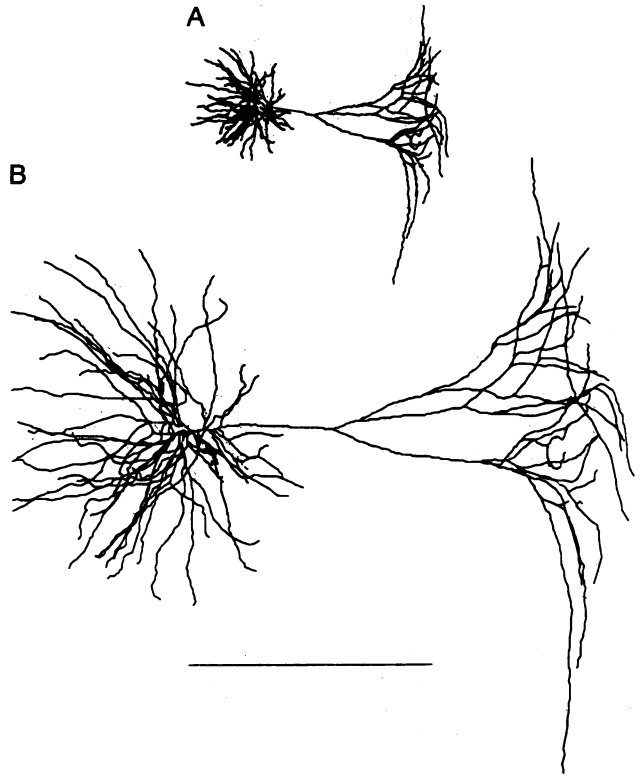

FIG. 3. Electrotonic size of the pyramidal cell. The electrotonic length for each branch was calculated and summed up to compute the electrotonic distance of each point to the soma (in dimensionless units). (*A*) In the absence of any background activity (i.e., $f = 0$), the cell is electrically very compact. This approximates the condition in a slice. (*B*) At $f = 2$ Hz, the effective membrane conductance $G_{m,eff}$ is much larger, decoupling the distal upper part of the apical tree from the cell body. Notice that this manner of plotting the functional geometry of cells, introduced by Zador *et al.* (23), emphasizes thin and long dendrites. The scale bar corresponds to 1 length constant, λ.

synaptic inputs needed to fire the cell for $f = 0$ compared to $f = 1$ is small (i.e., 113 vs. 115), in spite of the more than 5-fold decrease in somatic input resistance. The effect of the smaller size of the individual EPSP at higher values of f is compensated for by the fact that the resting potential of the cell has been shifted toward the firing threshold of the cell (about −49 mV). Finally, Fig. 4*B* compares the case of 150 synchronized versus unsynchronized synaptic inputs arriving repetitively with a 25-msec periodicity for $f = 1$ Hz. If the input is synchronized in time, seven out of eight cycles produce an action potential, whereas for the unsynchronized input, only a single spike is triggered—a compelling demonstration of the effect of synchronized input.

DISCUSSION

The principal phenomenon reported here is the dramatic effect the overall network activity can have on the spatiotemporal integration behavior of single neurons. The large decrease in R_{in}, τ_m, and other cellular parameters upon increasing f is contingent upon two assumptions: (*i*) that the input resistance in the absence of any afferent activity ($f = 0$) is high and (*ii*) that on the order of several thousand or more synaptic events occur per second. The decrease in these parameters does not depend on the particular details of the synaptic density, synaptic time course, reversal potential, and cellular geometry. Our results show that the large values of R_{in} and τ_m recently reported by several groups using patch-clamp techniques for cortical or hippocampal pyramidal cells under *in vitro* conditions (4, 5, 25) may simply reflect

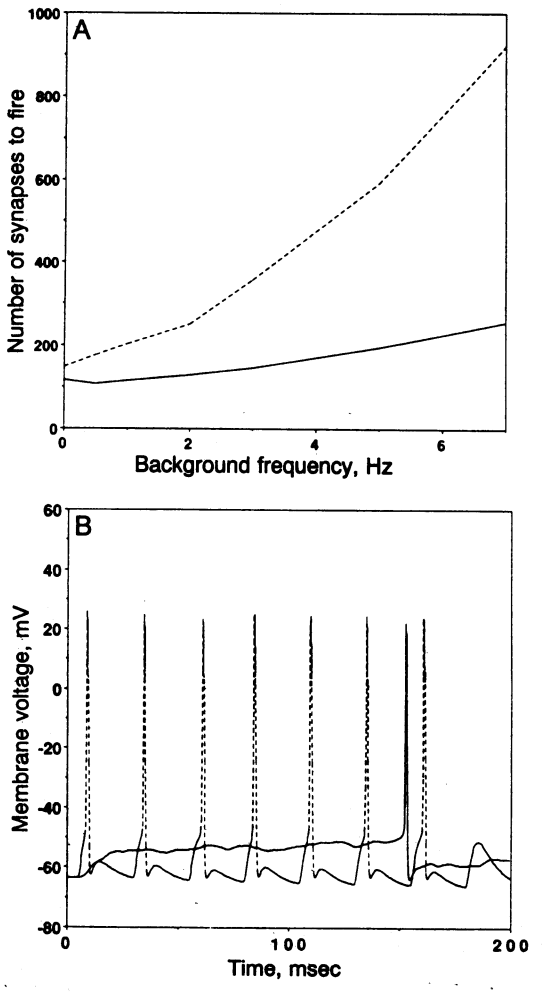

FIG. 4. Coincidence detection. A number of excitatory synapses were fired either simultaneously or spread out in time and were superimposed onto the synaptic background activity. The synapses were distributed throughout the cell. For the unsynchronized case, a Poisson process determined their activation times. (*A*) We plot here n, the minimum number of synapses (at $g_{peak} = 0.5$ nS) necessary to trigger a single action potential as a function of the background frequency, f. The lower curve (—) is for the case when all n synapses are activated simultaneously, while the upper curve (– – –) shows n when the activation times of the synapses are spread over 25 msec. On the abscissa, $f = 0$, 0.5, 1, 2, 3, 5, and 7 Hz corresponds to a G_{in} of 9.1, 49, 71, 84, 91, 123, and 151 nS, respectively. (*B*) The somatic potential when 150 excitatory synapses distributed throughout the cell are repeatedly activated at 40 Hz for eight cycles. If the input is synchronized (– – –) in time (that is, all 150 inputs are activated every 25 msec simultaneously), seven spikes are triggered, while only a single one is generated if the input is dispersed throughout the 25-msec interval (—). If the activation times of the 150 synapses are spread over the first 12.5 msec of every cycle, only two spikes are generated on average (not shown). The synaptic background frequency is $f = 1$ Hz.

the lack of general synaptic background activity typically observed in slice preparations. This also explains the more negative values of V_{rest} seen in slices as compared to *in vivo* intracellular recordings.

That a large difference between *in vivo* and *in vitro* recordings has not been observed earlier appears to be partially due to the impalement damage of the microelectrode recording technique used. In a careful study of this problem using the perforated patch-clamp technique, Spruston and Johnston (5) report 3–4 times higher values of R_{in} and 2–3 times higher values of τ_m in CA1 and CA3 pyramidal cells than measured with conventional microelectrodes. They explain this dis-

crepancy within a numerical model by introducing a somatic shunt caused by the electrode damage (see also ref. 26).

As pointed out previously by Holmes and Woody (7), synaptic activity can significantly change the effectiveness of individual inputs as well as the electrotonic structure of the cell. Thus, at $f = 0$, even the distal part of the apical tree in layer I has an equivalent electrotonic distance of no more than 1.2, while the distance increases by a factor of 2.5 for $f = 2$. In other words, input to the superficial layers of the tree becomes more and more decoupled from the soma as the overall network activity increases, with possibly interesting functional consequences for the feedback pathway from higher cortical areas preferentially terminating in the upper layers (27). However, as the coupling between individual synaptic input sites and the soma decreases as f is increased, a confounding effect is that the cell is pulled toward more positive potentials, bringing the cell closer to threshold. The extent to which one effect dominates the other depends on the details of the model.

In the temporal domain, the effect of varying f is quite clear. As f increases, the cell discriminates better between synaptic input arriving simultaneously than the same input spread out in time. As witnessed by Fig. 4, if between 100 and 200 synaptic inputs excite the cell, synchronized inputs, whether occurring only once or repetitively every 25 msec, lead to a response, whereas desynchronized input fails to trigger a spike. Thus, the cell acts as a coincidence detector whose tuning is enhanced as the general network activity increases. Note that we have here only considered the case in which the synaptic input is spread throughout the cell. Furthermore, the presence of massive synaptic input, such as during visual stimulation, will further briefly increase the dendritic input conductance, thereby reducing the effective time constant and increasing the sensitivity of the cell to temporal phase (see figure 11 in ref. 28). Our prediction is simple to test experimentally, by recording from one cell and varying the overall network activity with the help of sensory afferents or neurochemical substances. These results may have important implications for the relevance of temporal patterning of neuronal firing in cortex (29, 30) or for gain control in the face of varying visual contrast (T. Poggio, personal communication). Finally, our study illustrates how the overall activity of a neuronal network can alter the properties of the basic computational units underlying the network behavior.

Note. We recently learned that Rapp *et al.* (31) have independently studied this problem in the case of cerebellar Purkinje cells and have arrived at very similar conclusions.

We thank Tom Tromey for writing the graphics software; Mike Hines for providing us with NEURON; and Paul Bush, Francis Crick, Bill Lytton, Tomaso Poggio, Terrence Sejnowski, and Anthony Zador for discussion of these results. This work was supported by the Office of Naval Research, the National Science Foundation, the James S. McDonnell Foundation, and the International Human Frontier Science Program Organization. KACM is the Royal Society Henry Head Fellow.

1. Gilbert, C. (1977) *J. Physiol. (London)* **268,** 391–421.
2. Leventhal, A. G. & Hirsch, H. V. B. (1978) *J. Neurophysiol.* **41,** 948–962.
3. Larkman, A. U. (1991) *J. Comp. Neurol.* **306,** 332–343.
4. Major, G., Larkman, A. U. & Jack, J. J. B. (1990) *J. Physiol. (London)* **430,** 13P.
5. Spruston, N. & Johnston, D. (1991) *J. Neurophysiol.*, in press.
6. Barrett, J. N. (1975) *Fed. Proc. Fed. Am. Soc. Exp. Biol.* **34,** 1398–1407.
7. Holmes, W. R. & Woody, C. D. (1989) *Brain Res.* **505,** 12–22.
8. Douglas, R. J., Martin, K. A. C. & Whitteridge, D. (1991) *J. Physiol. (London)* **440,** 659–696.
9. Hines, M. (1989) *Int. J. Biomed. Comput.* **24,** 55–68.
10. Martin, K. A. C. (1988) *Q. J. Exp. Physiol.* **73,** 637–702.
11. Bekkers, J. M. & Stevens, C. F. (1989) *Nature (London)* **341,** 230–233.
12. Zador, A., Koch, C. & Brown, T. H. (1990) *Proc. Natl. Acad. Sci. USA* **87,** 6718–6722.
13. White, E. (1989) *Cortical Circuits* (Birkhaeuser, Boston).
14. Stratford, K., Mason, A., Larkman, A., Major, G. & Jack, J. J. B. (1989) in *The Computing Neuron*, eds. Durbin, R. Miall, C. & Michison, G. (Addison-Wesley, London).
15. Segev, I., Rapp, M., Manor, Y. & Yarom, Y. (1991) in *Single Neuron Computation*, eds. McKenna, T., Davis, J. & Zornetzer, S. F. (Academic, New York), in press.
16. Bush, P. & Douglas, R. J. (1991) *Neural Comp.* **3,** 19–30.
17. Stafstrom, C. E., Schwindt, P. C. & Crill, W. E. (1984) *J. Neurophysiol.* **52,** 264–277.
18. Douglas, R. J. & Martin, K. A. C. (1990) in *The Synaptic Organization of the Brain*, ed. Shepherd, G. M. (Oxford Univ. Press, New York), 3rd Ed.
19. Neher, E. (1970) Ph.D. thesis (University of Munich, Munich, F.R.G.).
20. Shelton, D. P. (1985) *Neuroscience* **14,** 111–131.
21. Connors, B. W. & Gutnick, M. J. (1990) *Trends Neurosci.* **13,** 99–104.
22. Mason, A., Nicoll, A. & Stratford, K. (1991) *J. Neurosci.* **11,** 72–84.
23. Zador, A. M., Claiborne, B. J. & Brown, T. H. (1991) *Soc. Neurosci. Abstr.* 605.6.
24. Koch, C., Poggio, T. & Torre, V. (1982) *Philos. Trans. R. Soc. London Ser. B* **298,** 227–264.
25. Anderson, P., Raastad, M. & Storm, J. F. (1990) *Cold Spring Harbor Symp. Quant. Biol.* **55,** 81–86.
26. Pongracz, F., Firestein, S. & Shepherd, G. M. (1991) *J. Neurophysiol.* **65,** 747–758.
27. Mignard, M. & Malpeli, J. G. (1991) *Science* **251,** 1249–1251.
28. Lytton, W. W. & Sejnowski, T. J. (1991) *J. Neurophysiol.* **66,** 1059–1079.
29. Gray, C. M., König, P., Engel, A. K. & Singer, W. (1989) *Nature (London)* **338,** 334–337.
30. Crick, F. & Koch, C. (1990) *Semin. Neurosci.* **2,** 263–275.
31. Rapp, M., Yarom, Y. & Segev, I. (1992) *Neural Comp.*, in press.